Article (Discoveries)

R2d2 drives selfish sweeps in the house mouse

John P Didion[1,2,3]*, Andrew P Morgan[1,2,3]*, Liran Yadgary[1,2,3], Timothy A Bell[1,2,3], Rachel C McMullan[1,2,3], Lydia Ortiz de Solorzano[1,2,3], Janice Britton-Davidian[4], Carol J Bult[5], Karl J Campbell[6,7], Riccardo Castiglia[8], Yung-Hao Ching[9], Amanda J Chunco[10], James J Crowley[1], Elissa J Chesler[5], John E French[11], Sofia I Gabriel[12], Daniel M Gatti[5], Theodore Garland Jr.[13], Eva B Giagia-Athanasopoulou[14], Mabel D Giménez[15], Sofia A Grize[16], İslam Gündüz[17], Andrew Holmes[18], Heidi C Hauffe[19], Jeremy S Herman[20], James M Holt[21], Kunjie Hua[1], Wesley J Jolley[22], Anna K Lindholm[16], María J López-Fuster[23], George Mitsainas[14], Maria da Luz Mathias[12], Leonard McMillan[21], M Graça Ramalhinho[23], Barbara Rehermann[24], Stephan P Rosshart[24], Jeremy B Searle[25], Meng-Shin Shiao[26], Emanuela Solano[8], Karen L Svenson[5], Pat Thomas-Laemont[10], David W Threadgill[27], Jacint Ventura[28], George M Weinstock[29], Daniel Pomp[1,3], Gary A Churchill[5], Fernando Pardo-Manuel de Villena[1,2,3]

1. Department of Genetics, University of North Carolina at Chapel Hill, Chapel Hill, NC, US

2. Lineberger Comprehensive Cancer Center, University of North Carolina at Chapel Hill, Chapel Hill, NC, US

3. Carolina Center for Genome Science, University of North Carolina at Chapel Hill, Chapel Hill, NC, US

4. Institut des Sciences de l'Evolution, Université de Montpellier, CNRS, IRD, EPHE, Montpellier, FR

5. The Jackson Laboratory, Bar Harbor, ME, US

6. Island Conservation, Puerto Ayora, Galápagos Island, EC

7. School of Geography, Planning & Environmental Management, The University of Queensland, St Lucia, AU

8. Department of Biology and Biotechnologies "Charles Darwin", University of Rome "La Sapienza", Rome, IT

9. Department of Molecular Biology and Human Genetics, Tzu Chi University, Hualien, TW

10. Department of Environmental Studies, Elon University, Elon, NC, US

11. National Toxicology Program, National Institute of Environmental Sciences, NIH, Research Triangle Park, NC, US

12. Department of Animal Biology & CESAM - Centre for Environmental and Marine Studies, Faculty of Sciences, University of Lisbon, Lisboa, PT

13. Department of Biology, University of California Riverside, Riverside, CA, US

14. Section of Animal Biology, Department of Biology, University of Patras, Patras, GR

15. Instituto de Biología Subtropical, CONICET - Universidad Nacional de Misiones, Posadas, MS, AR

16. Institute of Evolutionary Biology and Environmental Studies, University of Zurich, Zurich, CH

17. Department of Biology, Faculty of Arts and Sciences, University of Ondokuz Mayis, Samsun, TU

18. Laboratory of Behavioral and Genomic Neuroscience, National Institute on Alcohol Abuse and Alcoholism, NIH, Bethesda, MD, US

19. Department of Biodiversity and Molecular Ecology, Research and Innovation Centre, Fondazione Edmund Mach, S. Michele all'Adige, TN, IT

20. Department of Natural Sciences, National Museums Scotland, Edinburgh, UK

21. Department of Computer Science, University of North Carolina at Chapel Hill, Chapel Hill, NC, US

22. Island Conservation, Santa Cruz, CA, US

23. Faculty of Biology, Universitat de Barcelona, Avinguda Diagonal 643, 08028 Barcelona, ES

24. Immunology Section, Liver Diseases Branch, National Institute of Diabetes and Digestive and Kidney Diseases, NIH, Bethesda, MD, US

25. Department of Ecology and Evolutionary Biology, Cornell University, Ithaca, NY, US

26. Research Center, Faculty of Medicine, Ramathibodi Hospital, Mahidol University, 10400, Bangkok, TH

27. Department of Veterinary Pathobiology and Department of Molecular and Cellular Medicine, Texas A&M University, College Station, TX, US

28. Departament de Biologia Animal, de Biologia Vegetal i d'Ecologia, Facultat de Biociències, Universitat Autònoma de Barcelona, Barcelona, ES

29. Jackson Laboratory for Genomic Medicine, Farmington, CT, US

* These authors contributed equally to this work

Corresponding author: Fernando Pardo-Manuel de Villena, fernando@med.unc.edu

Abstract

A selective sweep is the result of strong positive selection driving newly occurring or standing genetic variants to fixation, and can dramatically alter the pattern and distribution of allelic diversity in a population. Population-level sequencing data have enabled discoveries of selective sweeps associated with genes involved in recent adaptations in many species. In contrast, much debate but little empirical evidence addresses whether "selfish" genes are capable of fixation – thereby leaving signatures identical to classical selective sweeps – despite being neutral or deleterious to organismal fitness. We previously described *R2d2*, a large copy-number variant that causes non-random segregation of mouse Chromosome 2 in females due to meiotic drive. Here we show population-genetic data consistent with a selfish sweep driven by alleles of *R2d2* with high copy number ($R2d2^{HC}$) in natural populations. We replicate this finding in multiple closed breeding populations from six outbred backgrounds segregating for *R2d2* alleles. We find that $R2d2^{HC}$ rapidly increases in frequency, and in most cases becomes fixed in significantly fewer generations than can be explained by genetic drift. $R2d2^{HC}$ is also associated with significantly reduced litter sizes in heterozygous mothers, making it a true selfish allele. Our data provide direct evidence of populations actively undergoing selfish sweeps, and demonstrate that meiotic drive can rapidly alter the genomic landscape in favor of mutations with neutral or even negative effects on overall Darwinian fitness. Further study will reveal the incidence of selfish sweeps, and will elucidate the relative contributions of selfish genes, adaptation and genetic drift to evolution.

Introduction

Population-level sequencing data have enabled analyses of positive selection in many species, including mice (Staubach et al. 2012) and humans (Williamson et al. 2007; Grossman et al. 2013; Colonna et al. 2014). These studies seek to identify genetic elements, such as single nucleotide variants (SNVs) and copy number variants (CNVs), that are associated with phenotypic differences

between populations that share a common origin (Fu and Akey 2013; Bryk and Tautz 2014). A marked difference in local genetic diversity between closely related taxa might indicate that one lineage has undergone a sweep, in which a variant under strong positive selection rises in frequency and carries with it linked genetic variation ("genetic hitch-hiking"), thereby reducing local haplotype diversity (Maynard Smith and Haigh 1974; Kaplan et al. 1989). In genomic scans for sweeps, it is typically assumed that the driving allele will have a strong positive effect on organismal fitness. Prominent examples of sweeps for which this assumption holds true (*i.e.* classic selective sweeps) include alleles at the *Vkorc1* locus, which confers rodenticide resistance in the brown rat (Pelz et al. 2005), and enhancer polymorphisms conferring lactase persistence in human beings (Bersaglieri et al. 2004). However, we and others have suggested that selfish alleles that strongly promote their own transmission irrespective of their effects on overall fitness could give rise to genomic signatures indistinguishable from those of classic selective sweeps (Sandler and Novitski 1957; White 1978; Henikoff and Malik 2002; Derome et al. 2004; Pardo-Manuel de Villena 2004; Brandvain and Coop 2011).

Suggestive evidence that sweeps may be driven by selfish alleles comes from studies in *Drosophila*. Incomplete sweeps have been identified at the *Segregation Distorter* (SD) locus (Presgraves et al. 2009) and in at least three X-chromosome systems (Babcock and Anderson 1996; Dyer et al. 2007; Derome et al. 2008; Kingan et al. 2010), all of which drive through the male germline. In addition, genomic conflict has been proposed as a possible driver of two nearly complete sweeps in *D. mauritiana* (Nolte et al. 2013). Incomplete sweeps were also detected in natural populations of *Mimulus* (monkeyflower), and the cause was identified as female meiotic drive of the centromeric *D* locus (Fishman and Saunders 2008). That all evidence of selfish sweeps derives from two genera is to some extent reflective of a selection bias, but may also indicate a difference in the incidence or effect of selfish alleles between these taxa and equally well-studied mammalian species (*e.g.* humans and mice). Furthermore, the lack of completed selfish sweeps reported in the literature may be due to an unexpected

130 strength of balancing selection, in which the deleterious effects of selfish alleles
131 prevent them from driving to fixation, or due to insufficient methods of detection.

132 Here, we investigate whether a selfish allele can sweep in natural and laboratory
133 populations of the house mouse, *M. m. domesticus.* We recently described *R2d2*,
134 a meiotic drive responder locus on mouse Chromosome 2 (Didion et al. 2015).
135 *R2d2* is a variably sized copy number gain of a 127 kb core element that
136 contains a single annotated gene, *Cwc22* (a spliceosomal protein). In females
137 heterozygous for *R2d2*, transmission of an allele with high copy number ($R2d2^{HC}$)
138 relative to an allele with low copy number ($R2d2^{LC}$) is a quantitative trait
139 controlled by multiple unlinked modifier loci. We define "high copy number" as the
140 minimum copy number with evidence of distorted transmission in existing
141 experiments – approximately 7 units of the core element. Distorted transmission
142 is present in some laboratory crosses (Siracusa et al. 1991; Montagutelli et al.
143 1996; Swallow et al. 1998; Eversley et al. 2010; Kelly et al. 2010a) segregating
144 for $R2d2^{HC}$ alleles, but absent in others (Didion et al. 2015). $R2d2^{HC}$ genotype is
145 also either uncorrelated or negatively correlated with litter size – a major
146 component of absolute fitness – depending on the presence of meiotic drive.
147 $R2d2^{HC}$ therefore behaves as a selfish genetic element. In the current study, we
148 provide evidence of a recent sweep at $R2d2^{HC}$ in wild *M. m. domesticus* mice,
149 and we show that $R2d2^{HC}$ has repeatedly driven selfish sweeps in closed-
150 breeding mouse populations.

151 Results and Discussion

152 *Evidence for a selfish sweep in wild mouse populations*

153 A recent study (Pezer et al. 2015) showed extreme copy number variation at
154 *Cwc22* in a sample of 26 wild mice (*M. m. domesticus*). To determine whether
155 this was indicative of *R2d2* copy number variation in the wild, we assayed an
156 additional 396 individuals sampled from 14 European countries and the United
157 States (**Supplementary Table 1** and **Figure 1**). We found that $R2d2^{HC}$ alleles

158 are segregating at a wide range of frequencies in natural populations (0.00 –
159 0.67; **Table 1**).

160 To test for a selfish sweep at *R2d2*^{HC}, we genotyped the wild-caught mice on the
161 MegaMUGA array (Rogala et al. 2014; Morgan and Welsh 2015; Morgan et al.
162 2015) and examined patterns of haplotype diversity. In the case of strong positive
163 selection, unrelated individuals are more likely to share extended segments
164 identical by descent (IBD) in the vicinity of the selected locus (Albrechtsen et al.
165 2010), compared with a population subject only to genetic drift. Consistent with
166 this prediction, we observed an extreme excess of shared IBD across
167 populations around *R2d2* (**Figure 2A**): *R2d2* falls in the top 0.25% of IBD-sharing
168 scores across the autosomes. In all cases, the shared haplotype has high copy
169 number, and this haplotype appears to have a single origin in European mice
170 (**Supplementary Figure 1**). Strong signatures are also evident at a previously
171 identified target of positive selection, the *Vkorc1* locus (distal Chromosome 7)
172 (Song et al. 2011).

173 In principle, the strength and age of a sweep can be estimated from the extent of
174 loss of genetic diversity around the locus under selection. From the SNP data,
175 we identified a ~1 Mb haplotype with significantly greater identity between
176 individuals with *R2d2*^{HC} alleles compared to the surrounding sequence. We used
177 published sequencing data from 26 wild mice (Pezer et al. 2015) to measure
178 local haplotype diversity around *R2d2* and found that the haplotypes associated
179 with *R2d2*^{HC} alleles are longer than those associated with *R2d2*^{LC} (**Figure 2B-C**).
180 This pattern of extended haplotype homozygosity is consistent with positive
181 selection over an evolutionary timescale as short as 450 generations (see
182 **Methods**). However, due to the extremely low rate of recombination in the
183 vicinity of *R2d2* (Didion et al. 2015), this is most likely an underestimate of the
184 true age of the mutation.

185 It is important to note that the excess IBD we observe at *R2d2* (**Figure 2A**) arises
186 from segments shared *between* geographically distinct populations (**Figure 1**).
187 When considering sharing *within* populations only (**Supplementary Figure 2**),

188 *R2d2* is no longer an outlier. Therefore, it was unsurprising that we failed to
189 detect a sweep around *R2d2* using statistics that are designed to identify
190 population-specific differences in selection, like hapFLK (Fariello et al. 2013), or
191 selection in aggregate, like iHS (Voight et al. 2006) (**Supplementary Figure 3**).

192 ***A selfish sweep in an outbred laboratory population***

193 We validated the ability of $R2d2^{HC}$ to drive a selfish sweep by examining *R2d2*
194 allele frequencies in multiple closed-breeding laboratory populations for which we
195 had access to samples from the founder populations. The Diversity Outbred (DO)
196 is a randomized outbreeding population derived from eight inbred mouse strains
197 that is maintained under conditions designed to minimize the effects of both
198 selection and genetic drift (Svenson et al. 2012). Expected time to fixation or loss
199 of an allele present in the founder generation (with initial frequency 1/8) is ~900
200 generations. The WSB/EiJ founder strain contributed an $R2d2^{HC}$ allele which
201 underwent a more than three-fold increase (from 0.18 to 0.62) in 13 generations
202 ($p < 0.001$ by simulation; range 0.03 – 0.26 after 13 generations in 1000
203 simulation runs) (**Figure 3A**), accompanied by significantly distorted allele
204 frequencies ($p < 0.01$ by simulation) across a ~100 Mb region linked to the allele
205 (**Figure 3B**).

206 **$R2d2^{HC}$** ***has an underdominant effect on fitness***

207 The fate of a selfish sweep depends on the fitness costs associated with the
208 different genotypic classes at the selfish genetic element. For example,
209 maintenance of intermediate frequencies of the *t*-complex (Lyon 1991) and *SD*
210 (Hartl 1973) chromosomes in natural populations of mice and *Drosophila*,
211 respectively, is thought to result from decreased fecundity associated with those
212 selfish elements.

213 To assess the fitness consequences of $R2d2^{HC}$ we treated litter size as a proxy
214 for absolute fitness (**Figure 3C**). We determined whether each female had
215 distorted transmission of *R2d2* using a one-sided exact binomial test for deviation
216 from the expected Mendelian genotype frequencies in her progeny. Average litter
217 size among DO females homozygous for $R2d2^{LC}$ ("LL" in Figure 3C: 8.1; 95% CI

218 7.8 – 8.3) is not different than among females homozygous for *R2d2*^{HC} ("HH":
219 8.1; 95% CI 7.4 – 8.9) or among heterozygous females without distorted
220 transmission of *R2d2*^{HC} ("LH-TRD": 8.1; 95% CI 7.7 – 8.5). However, in the
221 presence of meiotic drive, litter size is markedly reduced ("LH+TRD": 6.5; 95% CI
222 5.9 – 7.2; $p = 5.7 \times 10^{-5}$ for test of difference versus all other classes). The
223 relative fitness of heterozygous females with distorted transmission is $w = 0.81$,
224 for a selection coefficient of $s = 1 - w = 0.19$ (95% CI 0.10 – 0.23) against the
225 heterozygote. Despite this underdominant effect, the absolute number of *R2d2*^{HC}
226 alleles transmitted by heterozygous females in each litter is significantly higher in
227 the presence of meiotic drive than its absence ($p = 0.032$; **Figure 3D**). The rising
228 frequency of *R2d2*^{HC} in the DO thus represents a truly selfish sweep.

229 ***Selfish sweeps in other laboratory populations***

230 We also observed selfish sweeps in selection lines derived from the ICR:Hsd
231 outbred population (Swallow et al. 1998), in which *R2d2*^{HC} alleles are segregating
232 (**Figure 4A**). Three of four lines selectively bred for high voluntary wheel-running
233 (HR lines) and two of four control lines (10 breeding pairs per line per generation
234 in both conditions) went from starting *R2d2*^{HC} frequencies ~0.75 to fixation in 60
235 generations or less: two lines were fixed by generation 20, and three more by
236 generation 60. In simulations mimicking this breeding design and neutrality
237 (**Figure 4B**), median time to fixation was 46 generations (5th percentile: 9
238 generations). Although the *R2d2*^{HC} allele would be expected to eventually fix by
239 drift in 6 of 8 lines given its high starting frequency, fixation in two lines within 20
240 generations and three more lines by 60 generations is not expected ($p = 0.003$ by
241 simulation). In a related advanced intercross segregating for high and low copy
242 number alleles at *R2d2* (HR8xC57BL/6J (Kelly et al. 2010b)), we observed that
243 *R2d2*^{HC} increased from a frequency of 0.5 to 0.85 in just 10 generations and fixed
244 by 15 generations (**Figure 4C**), versus a median 184 generations in simulations
245 ($p < 0.001$; **Figure 4D**). The increase in *R2d2*^{HC} allele frequency in the DO and
246 the advanced intercross populations occurred at least an order of magnitude
247 faster than what is predicted by drift alone.

248 Using archival tissue samples, we were able to determine *R2d2* allele
249 frequencies in the original founder populations of 6 of the ~60 wild-derived inbred
250 strains available for laboratory use (Didion and Pardo-Manuel de Villena 2013).
251 In four strains, WSB/EiJ, WSA/EiJ, ZALENDE/EiJ, and SPRET/EiJ, $R2d2^{HC}$
252 alleles were segregating in the founders and are now fixed in the inbred
253 populations. In the other two strains, LEWES/EiJ and TIRANO/EiJ, the founders
254 were not segregating for *R2d2* copy number and the inbred populations are fixed,
255 as expected, for $R2d2^{LC}$ (**Supplementary Figure 4**). This trend in wild-derived
256 strains is additional evidence of the tendency for $R2d2^{HC}$ to go to fixation in
257 closed breeding populations when segregating in the founder individuals.

258 ***On the distribution and frequency of* R2d2^{HC} *alleles in the wild***

259 Considering the degree of transmission distortion in favor of $R2d2^{HC}$ (up to 95%
260 (Didion et al. 2015)), and that $R2d2^{HC}$ repeatedly goes to fixation in laboratory
261 populations, the moderate frequency of $R2d2^{HC}$ in the wild (0.14 worldwide,
262 **Table 1**) is initially surprising. Neither do we find any obvious association
263 between geography and $R2d2^{HC}$ allele frequency that might indicate the
264 mutation's origin or its pattern of gene flow (**Table 1** and **Figure 1**).

265 Several observations may explain these results. First, relative to the effective
266 size of *M. m. domesticus* (82,500-165,000 (Geraldes et al. 2011)), our sample
267 size was small. Our sampling was also geographically sparse and non-uniform.
268 Thus, our allele frequency estimates may differ substantially from the true
269 population allele frequencies at *R2d2*.

270 Second, the reduction in litter size associated with $R2d2^{HC}$ may have a greater
271 impact on *R2d2* allele frequency in a natural population than in the controlled
272 laboratory populations we studied. In these breeding schemes each mating pair
273 contributes the same number of offspring to the next generation so that most
274 fitness differences are effectively erased.

275 Third, $R2d2^{HC}$ alleles may be unstable and lose the ability to drive upon reverting
276 to low copy number. This has been reported previously (Didion et al. 2015).

277 Fourth, in an large population (*i.e.* in the wild) the dynamics of an underdominant
278 meiotic drive allele are only dependent on the relationship between the degree of
279 transmission distortion (m) and the strength of selection against heterozygotes
280 (Hedrick 1981) (s). This relationship can be expressed by the quantity q (see
281 **Methods**), for which $q > 1$ indicates increasing probability of fixation of the driving
282 allele, $q < 1$ indicates increasing probability that the allele will be purged, and $q \approx$
283 1 leads to maintenance of the allele at an (unstable) equilibrium frequency. The
284 fate of the driving allele in a finite population additionally depends on the
285 population size (Hedrick 1981): the smaller the population, the greater the
286 likelihood that genetic drift will fix a mutation with $q < 1$ (**Figure 5A-B**). We note
287 that $R2d2^{HC}$ appears to exist close to the $q \approx 1$ boundary ($s \approx 0.2$, $m \approx 0.7$, and
288 thus $q \approx 0.96$).

289 Last but not least, in contrast to many meiotic drive systems, in which the
290 component elements are tightly linked, the action of $R2d2^{HC}$ is dependent on
291 unlinked modifier loci whose frequencies, modes of action, and effect sizes are
292 unknown. It is therefore difficult to predict the effect of the modifiers on *R2d2*
293 allele frequencies in the wild. We used forward-in-time simulations to explore the
294 effect of a single unlinked modifier locus on fixation probability of a driving allele.
295 Under an additive model ($m = 0.80$ for modifier genotype *AA*, 0.65 for genotype
296 *Aa* and 0.50 for genotype *aa*), fixation probability is reduced and time to fixation
297 is increased by the presence of the modifier locus (**Figure 5C-D**). As the modifier
298 allele becomes more rare, fixation probability approaches the neutral expectation
299 ($1/2N$, where N is population size). Importantly, the driving allele tends to sweep
300 until the modifier allele is lost, and then drifts either to fixation or loss (**Figure**
301 **5E**). Drift at modifier loci thus creates a situation akin to selection in a varying
302 environment – one outcome of which is balancing selection (Gillespie 2010). This
303 is consistent with the maintenance of $R2d2^{HC}$ at intermediate frequencies in
304 multiple populations separated by space and time, as we observe in wild mice.

305 ***Concluding remarks***

306 Most analyses of positive selection in the literature assume that the likelihood of
307 a newly arising mutation becoming established, increasing in frequency and even
308 going to fixation within a population is positively correlated with its effect on
309 organismal fitness. Here, we have shown that a selfish genetic element has
310 repeatedly driven sweeps in which the change in allele frequency and the effect
311 on organismal fitness are decoupled. Our results suggest that evolutionary
312 studies should employ independent evidence to determine whether loci
313 implicated as drivers of selective sweeps are adaptive or selfish.

314 Although a selfish sweep has clear implications for such experimental
315 populations as the DO and the Collaborative Cross (Didion et al. 2015), the
316 larger evolutionary implications of selfish sweeps are less obvious. On the one
317 hand, sweeps may be relatively rare, as appears to be the case for classic
318 selective sweeps in recent human history (Hernandez et al. 2011). On the other
319 hand, theory and comparative studies indicate that selfish genetic elements may
320 be a potent force during speciation (White 1978; Hedrick 1981; Pardo-Manuel de
321 Villena and Sapienza 2001; Henikoff and Malik 2002; Brandvain and Coop 2011).
322 With the growing appreciation for the potential importance of non-Mendelian
323 genetics in evolution, and the increasing tractability of population-scale genetic
324 analyses, we anticipate that the effects of selfish elements such as *R2d2* in
325 natural populations, including their contributions to events of positive selection,
326 will soon be elucidated.

327 Improved understanding of the mechanism of meiotic drive at *R2d2* may also
328 enable practical applications of selfish genetic elements. As demonstrated by the
329 recent use of RNA-guided genome editing to develop gene drive systems in
330 mosquitos and fruit flies (Esvelt et al. 2014; Gantz and Bier 2015; Hammond et
331 al. 2015), experimental manipulation of chromosome segregation is now feasible.
332 *R2d2* is an attractive option for the development of a mammalian gene drive
333 system because, as we have shown here, it has already proven capable of
334 driving to fixation in multiple independent genetic backgrounds. Furthermore,

335 there are multiple unlinked modifiers of *R2d2* that, when identified, might be
336 exploited for fine-grained manipulation of transmission ratios.

337 Materials and Methods

338 *Mice*

339 Wild *M. m. domesticus* mice were trapped at a large number of sites across
340 Europe and the Americas (**Figure 1A** (upper panel)**, and Supplementary Table**
341 **1**). A set of 29 *M. m. castaneus* mice trapped in northern India and Taiwan
342 (**Figure 1A**, lower panel) were included as an outgroup (Yang et al. 2011).
343 Trapping was carried out in concordance with local laws, and either did not
344 require approval or was carried out with the approval of the relevant regulatory
345 bodies (depending on the locality and institution).

346 All Diversity Outbred (DO) mice were bred at The Jackson Laboratory. Litter
347 sizes were counted within 24 hours of birth. Individual investigators purchased
348 mice for unrelated studies and contributed either tissue samples or genotype
349 data to this study (**Supplementary Table 2**).

350 High running (HR) selection and intercross lines were developed as previously
351 described (Swallow et al. 1998; Kelly et al. 2010a; Leamy et al. 2012). Mouse
352 tails were archived from 3 generations of the HR selection lines (-2, +22, and
353 +61) and from every generation of the HR8xC57BL/6J advanced intercross.

354 Progenitors of wild-derived strains have various origins (see **Supplementary**
355 **Methods**), and were sent to Eva M. Eicher at The Jackson Laboratory for
356 inbreeding in the early 1980s. Frozen tissues from animals in the founder
357 populations were maintained at The Jackson Laboratory by Muriel Davidson until
358 2014, when they were transferred to the Pardo-Manuel de Villena laboratory at
359 the University of North Carolina at Chapel Hill.

360 All laboratory mice were handled in accordance with the IACUC protocols of the
361 investigators' respective institutions.

362 ***Genotyping***

363 *Microarray genotyping and quality control:* Whole-genomic DNA was isolated
364 from tail, liver, muscle or spleen using Qiagen Gentra Puregene or DNeasy
365 Blood & Tissue kits according to the manufacturer's instructions. All genome-
366 wide genotyping was performed using the Mouse Universal Genotyping Array
367 (MUGA) and its successor, MegaMUGA (GeneSeek, Lincoln, NE) (Collaborative
368 Cross Consortium 2012; Morgan and Welsh 2015). Genotypes were called using
369 Illumina BeadStudio (Illumina Inc., Carlsbad, CA). We excluded all markers and
370 all samples with missingness greater than 10%. We also computed the sum
371 intensity for each marker: $S_i = X_i + Y_i$, where X_i and Y_i are the normalized
372 hybridization intensities of the two allelic probes. We determined the expected
373 distribution of sum intensity values using a large panel of control samples. We
374 excluded any array for which the set of intensities $I = \{S_1, S_2, \ldots, S_n\}$ was not
375 normally distributed or whose mean was significantly left-shifted from the
376 reference distribution (one-tailed *t*-test with $p < 0.05$).

377 *PCR genotyping:* The *R2d2* element has been mapped to a 900 kb critical region
378 on Chromosome 2: 83,631,096 – 84,541,308 (mm9 build), referred to herein as
379 the "candidate interval" (Didion et al. 2015). We designed primers to amplify two
380 regions within the candidate interval. *Primer Set A* targets a 318 bp region (chr2:
381 83,673,604 – 83,673,921) with two distinct haplotypes in linkage with either the
382 $R2d2^{LC}$ allele or the $R2d2^{HC}$ allele: 5'-CCAGCAGTGATGAGTTGCCATCTTG-3'
383 (forward) and 5'- TGTCACCAAGGTTTTCTTCCAAAGGGAA-3' (reverse). *Primer*
384 *Set B* amplifies a 518 bp region (chr2: 83,724,728 – 83,725,233); the amplicon is
385 predicted, based on whole-genome sequencing, to contain a 169 bp deletion in
386 HR8 relative to the C57BL/6J reference genome: 5'-
387 GAGATTTGGATTTGCCATCAA-3' (forward) and 5'-
388 GGTCTACAAGGACTAGAAACAG-3' (reverse). Primers were designed using
389 IDT PrimerQuest (https://www.idtdna.com/Primerquest/Home/Index).

390 Crude whole-genomic DNA for PCR reactions was extracted from mouse tails.
391 The tissues were heated in 100 µl of 25 mM NaOH/0.2 mM EDTA at 95°C for 60

392 minutes followed by the addition of 100 µl of 40 mM Tris-HCl. The mixture was
393 then centrifuged at 2000 x *g* for 10 minutes and the supernatant used as PCR
394 template. PCR reactions contained 1 µL dNTPs, 0.3 µL of each primer, 5.3 µL of
395 water, and 0.1 µL of GoTaq polymerase (Promega) in a final volume of 10 µL.
396 Cycling conditions were 95°C, 2-5 min, 35 cycles at 95°, 55° and 72°C for 30 sec
397 each, with a final extension at 72°C, 7 min.

398 For *Primer Set A*, products were sequenced at the University of North Carolina
399 Genome Analysis Facility on an Applied Biosystems 3730XL Genetic Analyzer.
400 Chromatograms were analyzed with the Sequencher software package (Gene
401 Codes Corporation, Ann Arbor, Michigan, United States). For *Primer Set B,*
402 products were visualized and scored on 2% agarose gels. Assignment to
403 haplotypes was validated by comparing the results to qPCR assays for the single
404 protein-coding gene within *R2d2*, *Cwc22* (see "Copy-number assays" below). For
405 generation +61, haplotypes were assigned based on MegaMUGA genotypes and
406 validated by the normalized per-base read depth from whole-genome sequencing
407 (see below), calculated with samtools mpileup (Li et al. 2009). The concordance
408 between qPCR, read depth, and haplotypes assigned by MegaMUGA or Sanger
409 sequencing is shown in **Supplementary Figure 5**.

410 *Assays:* Wild mice were genotyped on MegaMUGA (**Supplementary Table 1**).
411 DO mice were genotyped on MUGA and MegaMUGA (**Supplementary Table 2**).
412 HR selection lines were genotyped at three generations, one before (-2) and two
413 during (+22 and +61) artificial selection. We genotyped 185 randomly selected
414 individuals from generation -2 and 157 individuals from generation +22 using
415 *Primer Set A*. An additional 80 individuals from generation +61 were genotyped
416 with the MegaMUGA array (see "Microarray genotyping and quality-control"
417 below). The HR8xC57BL/6J advanced intercross line was genotyped with *Primer*
418 *Set B* in tissues from breeding stock at generations 3, 5, 8, 9, 10, 11, 12, 13, 14,
419 and 15.

420 ***Copy-number assays and assignment of* R2d2 *status.*** Copy-number at *R2d2*
421 was determined by qPCR for *Cwc22*, the single protein-coding gene in the *R2d*

422 repeat unit, as described in detail in (Didion et al. 2015). Briefly, we used
423 commercially available TaqMan kits (Life Technologies assay numbers
424 Mm00644079_cn and Mm00053048_cn) to measure the copy number of *Cwc22*
425 relative to the reference genes *Tfrc* (cat. no. 4458366, for target
426 Mm00053048_cn) or *Tert* (cat. no. 4458368, for target Mm00644079_cn). Cycle
427 thresholds (C_t) were determined for each target using ABI CopyCaller v2.0
428 software with default settings, and relative cycle threshold was calculated as

$$\Delta C_t = C_t^{reference} - C_t^{target}$$

429 We normalized the ΔC_t across batches by fitting a linear mixed model with batch
430 and target-reference pair as random effects.

431 Estimation of integer diploid copy numbers > ~3 by qPCR is infeasible without
432 many technical and biological replicates, especially in the heterozygous state.
433 We took advantage of *R2d2* diploid copy-number estimates from whole-genome
434 sequencing for the inbred strains C57BL/6J (0), CAST/EiJ (2) and WSB/EiJ (66),
435 and the (WSB/EiJxC57BL/6J)F_1 (33) to establish a threshold for declaring a
436 sample "high-copy." For each of the two TaqMan target-reference pairs we
437 calculated the sample mean ($\hat{\mu}$) and standard deviation ($\hat{\sigma}$) of the normalized ΔC_t
438 among CAST/EiJ controls and wild *M. m. castaneus* individuals together. We
439 designated as "high-copy" any individual with normalized ΔC_t greater than $\hat{\mu} + 2\hat{\sigma}$
440 – that is, any individual with approximately > 95% probability of having diploid
441 copy number >2 at *R2d2*. Individuals with high copy number and evidence of
442 local heterozygosity (a heterozygous call at any of the 13 markers in the *R2d2*
443 candidate interval) were declared heterozygous $R2d2^{HC/LC}$, and those with high
444 copy number and no heterozygous calls in the candidate interval were declared
445 homozygous $R2d2^{HC/HC}$.

446 ***Exploration of population structure in wild mice.***

447 Scans for signatures of positive selection based on patterns of haplotype-sharing
448 assume that individuals are unrelated. We identified pairs of related individuals
449 using the *IBS2** ratio (Stevens et al. 2011), defined as *HETHET / (HOMHOM +*

450 *HETHET)*, where *HETHET* and *HOMHOM* are the count of non-missing markers
451 for which both individuals are heterozygous (share two alleles) and homozygous
452 for opposite alleles (share zero alleles), respectively. Pairs with *IBS2** < 0.75
453 were considered unrelated. Among individuals which were a member of one or
454 more unrelated pairs, we iteratively removed one sample at a time until no
455 related pairs remained, and additionally excluded markers with minor-allele
456 frequency < 0.05 or missingness > 0.10. The resulting dataset contains
457 genotypes for 396 mice at 58,283 markers.

458 Several of our analyses required that samples be assigned to populations.
459 Because mice in the wild breed in localized demes and disperse only over short
460 distances (on the order of hundreds of meters) (Pocock et al. 2005), it is
461 reasonable to delineate populations on the basis of geography. We assigned
462 samples to populations based on the country in which they were trapped. To
463 confirm that these population labels correspond to natural clusters we performed
464 two exploratory analyses of population structure. First, classical multidimensional
465 scaling (MDS) of autosomal genotypes was performed with PLINK (Purcell et al.
466 2007) (--mdsplot --autosome). The result is presented in **Figure 1B-C**, in which
467 samples are colored by population. Second, we used TreeMix (Pickrell and
468 Pritchard 2012) to generate a population tree allowing for gene flow using the set
469 of unrelated individuals. Autosomal markers were first pruned to reach a set in
470 approximate linkage equilibrium (plink --indep 25 1). TreeMix was run on the
471 resulting set using the *M. m. castaneus* samples as an outgroup and allowing up
472 to 10 gene-flow edges (treemix -root "cas" -k 10) (**Figure 1D**). The clustering of
473 samples by population evident by MDS and the absence of long-branch
474 attraction in the population tree together indicate that our choices of population
475 labels are biologically reasonable.

476 ***Scans for selection in wild mice.*** Two complementary statistics, hapFLK
477 (Fariello et al. 2013) and standardized iHS score (Voight et al. 2006), were used
478 to examine wild-mouse genotypes for signatures of selection surrounding *R2d2*.
479 The hapFLK statistic is a test of differentiation of local haplotype frequencies
480 between hierarchically-structured populations. It can be interpreted as a

481 generalization of Wright's F_{ST} which exploits local LD. Its model for haplotypes is
482 that of fastPHASE (Scheet 2006) and requires a user-specified value for the
483 parameter *K*, the number of local haplotype clusters. We computed hapFLK in
484 the set of unrelated individuals using *M. m. castaneus* samples as an outgroup
485 for *K* = {4, 8, 12, 16, 20, 24, 28, 32} (hapflk --outgroup "cas" -k {K}) and default
486 settings otherwise.

487 The iHS score (and its allele-frequency-standardized form |iHS|) is a measure of
488 extended haplotype homozygosity on a derived haplotype relative to an ancestral
489 one. For consistency with the hapFLK analysis, we used fastPHASE on the same
490 genotypes over the same range of *K* with 10 random starts and 25 iterations of
491 expectation-maximization (fastphase –K{K} -T10 -C25) to generate phased
492 haplotypes. We then used selscan (Szpiech and Hernandez 2014) to compute
493 iHS scores (selscan --ihs) and standardized the scores in 25 equally-sized bins
494 (selscan-norm --bins 25).

495 Values in the upper tail of the genome-wide distribution of hapFLK or |iHS|
496 represent candidates for regions under selection. We used percentile ranks
497 directly and did not attempt to calculate approximate or empirical *p*-values.

498 ***Detection of identity-by-descent (IBD) in wild mice.*** As an alternative test for
499 selection, we computed density of IBD-sharing using the RefinedIBD algorithm of
500 BEAGLE v4.0 (r1399) (Browning and Browning 2013), applying it to the full set of
501 500 individuals. The haplotype model implemented in BEAGLE uses a tuning
502 parameter (the "scale" parameter) to control model complexity: larger values
503 enforce a more parsimonious model, increasing sensitivity and decreasing
504 computational cost at the expense of accuracy. The authors recommend a value
505 of 2.0 for ~1M SNP arrays in humans. We increased the scale parameter to 5.0
506 to increase detection power given (a) our much sparser marker set, and (b) the
507 relatively weaker local LD in mouse versus human populations (Laurie et al.
508 2007). We trimmed one marker from the ends of candidate IBD segments to
509 reduce edge effects (java -jar beagle.jar ibd=true ibdscale=5 ibdtrim=1). We
510 retained those IBD segments shared between individuals in the set of 396

511 unrelated mice. In order to limit noise from false-positive IBD segments, we
512 further removed segments with LOD score < 5.0 or width < 0.5 cM.

513 An empirical IBD-sharing score was computed in 500 kb bins with 250 kb overlap
514 as:

$$f_n = \frac{\sum_n s_{ij} p_{ij}}{w_{ij}}$$

515 where the sum in the numerator is taken over all IBD segments overlapping bin *n*
516 and s_{ij} is an indicator variable which takes the value 1 if individuals *i,j* share a
517 haplotype IBD in bin *n* and 0 otherwise. The weighting factor w_{ij} is defined as

$$w_{ij} = 0.001 \times \left(\frac{n_a n_b}{W}\right)^{1/2}$$

518 with

$$W = \max(n_a n_b)$$

519 where n_a and n_b are the number of unrelated individuals in the population to
520 which individuals *i* and *j* belong, respectively. This weighting scheme accounts
521 for the fact that we oversample some geographic regions (for instance, Portugal
522 and Maryland) relative to others. To explore differences in haplotype-sharing
523 within versus between populations we introduce an additional indicator p_{ij}. Within-
524 population sharing is computed by setting p_{ij} = 1 if individuals *i,j* are drawn from
525 the same population and p_{ij} = 0 otherwise. Between-population sharing is
526 computed by reversing the values of p_{ij}. The result is displayed in **Figure 2**.

527 ***Analysis of local sequence diversity in whole-genome sequence from wild***
528 ***mice.*** We obtained raw sequence reads for 26 unrelated wild mice (European
529 Nucleotide Archive project accession PRJEB9450 (Pezer et al. 2015)); samples
530 are listed in **Supplementary Table 3**. Details of the sequencing protocol are
531 given in the indicated reference. Briefly, paired-end libraries with mean insert size
532 230 bp were prepared from genomic DNA using the Illumina TruSeq kit. Libraries
533 were sequenced on the Illumina HiSeq 2000 platform with 2x100bp reads to an
534 average coverage of 20X per sample (populations AHZ, CLG and FRA) or 12X

535 per sample (population HGL). We realigned the raw reads to the mouse
536 reference genome (GRCm38/mm10 build) using BWA MEM (Li and Durban,
537 unpublished) with default parameters. SNPs relative to the reference sequence
538 of Chromosome 2 were called using samtools mpileup v0.1.19-44428cd with
539 maximum per-sample depth of 200. Genotype calls with root-mean-square
540 mapping quality < 30 or genotype quality > 20 were treated as missing. Sites
541 were used for phasing if they had a minor-allele count ≥ 2 and at most 2 missing
542 calls. BEAGLE v4.0 (r1399) was used to phase the samples conditional on each
543 other, using 20 iterations for phasing and default settings otherwise (java -jar
544 beagle.jar phasing-its=20). Sites were assigned a genetic position by linear
545 interpolation on the most recent genetic map for the mouse (Liu et al. 2010; Liu
546 et al. 2014).

547 The *R2d2* candidate interval spans positions 83,790,939 – 84,701,151 in the
548 mm10 reference sequence. As the index SNP for *R2d2*^{HC} we chose the SNP with
549 strongest nominal association with *R2d2* copy number (as estimated by Pezer *et*
550 *al.* (2015)) within 1 kb of the proximal boundary of the candidate interval. That
551 SNP is chr2:83,790,275T>C. The C allele is associated with high copy number
552 and is therefore presumed to be the derived allele. We computed the extended
553 haplotype homozygosity (EHH) statistic (Sabeti et al. 2002) in the phased dataset
554 over a 1 Mb window on each side of the index SNP using selscan (selscan --ehh
555 --ehh-win 1000000). The result is presented in **Figure 2B**. Decay of haplotypes
556 away from the index SNP was visualized as a bifurcation diagram (**Figure 2C**)
557 using code adapted from the R package rehh (https://cran.r-
558 project.org/package=rehh).

559 ***Estimation of age of* R2d2^{HC} *alleles in wild mice.*** To obtain a lower bound for
560 the age of *R2d2*^{HC} and its associated haplotype, we used the method of
561 Stephens *et al.* (1998) (Stephens et al. 1998). Briefly, this method approximates
562 the probability *P* that a haplotype is affected by recombination or mutation during
563 the *G* generations since its origin as

$$P = e^{-G(-\mu+r)}$$

564 where μ and r are the per-generation rates of mutation and recombination,
565 respectively. Assuming $\mu << r$ and, taking P', the observed number of ancestral
566 (non-recombined) haplotypes in a sample, as an estimator of P, obtain the
567 following expression for G:

$$G \approx -(\log P')/r$$

568 We enumerated haplotypes in our sample of 52 chromosomes at 3 SNPs
569 spanning the *R2d2* candidate interval. The most proximal SNP is the index SNP
570 for the EHH analyses (chr2:83,790,275T>C); the most distal SNP is the SNP
571 most associated with copy number within 1 kbp of the boundary of the candidate
572 interval (chr2:84,668,280T>C); and the middle SNP was randomly-chosen to fall
573 approximately halfway between (chr2:84,079,970C>T). The three SNPs span
574 genetic distance 0.154 cM (corresponding to r = 0.00154). The most common
575 haplotype among samples with high copy number according to Pezer et al.
576 (2015) was assumed to be ancestral. Among 52 chromosomes, 22 carried at
577 least part of the $R2d2^{HC}$-associated haplotype; of those, 11 were ancestral and
578 11 recombinant (**Supplementary Table 3**). This gives an estimated age of 450
579 generations for $R2d2^{HC}$.

580 We note that the approximations underlying this model assume constant
581 population size and neutrality. To the extent that haplotype homozygosity decays
582 more slowly on a positively- (or selfishly-) selected haplotype, we will
583 underestimate the true age of $R2d2^{HC}$.

584 ***Inference of local phylogeny at* R2d2*.*** To determine whether the $R2d2^{HC}$
585 haplotype(s) shared among wild mice have a single origin, we constructed a
586 phylogenetic tree from the 39 MegaMUGA SNPs in the region flanking *R2d2*
587 (Chromosome 2: 82 – 85 Mb). We first excluded individuals heterozygous in the
588 region and then constructed a matrix of pairwise distances from the proportion of
589 alleles shared identical-by-state (IBS) between samples. A tree was inferred from
590 the distance matrix using the neighbor-joining method implemented in the R
591 package ape (http://cran.r-project.org/package=ape).

592 ***Haplotype frequency estimation in the Diversity Outbred.*** We inferred the

593 haplotypes of DO individuals using probabilistic methods (Liu et al. 2010; Liu et
594 al. 2014). We combined the haplotypes of DO individuals genotyped in this study
595 with the Generation 8 individuals in Didion *et al.* (2015). As an additional QC
596 step, we computed the number of historical recombination breakpoints per
597 individual per generation (Svenson et al. 2012) and removed outliers (more than
598 1.5 standard deviations from the mean). We also excluded related individuals
599 based on the distribution of haplotype sharing between related and unrelated
600 individuals computed from simulations (mean 0.588 ± 0.045 for first-degree
601 relatives; mean 0.395 ± 0.039 for second-degree relatives; and mean 0.229 ±
602 0.022 for unrelated individuals; see **Supplementary Methods**). Finally, we
603 computed in each generation the frequency of each founder haplotype at 250 kb
604 intervals surrounding the *R2d2* region (Chromosome 2: 78-86 Mb), and identified
605 the greatest WSB/EiJ haplotype frequency.

606 ***Analyses of fitness effects of* R2d2^{HC} *in the Diversity Outbred.*** To assess the
607 consequences of *R2d2*^{HC} for organismal fitness, we treated litter size as a proxy
608 for absolute fitness. Using breeding data from 475 females from DO generations
609 13, 16, 18 and 19, we estimated mean litter size in four genotype groups:
610 females homozygous *R2d2*$^{LC/LC}$; females heterozygous *R2d2*$^{HC/LC}$ with
611 transmission ratio distortion (TRD) in favor of the *R2d2*^{HC} allele; females
612 heterozygous *R2d2*$^{HC/LC}$ without TRD; and females homozygous *R2d2*$^{HC/HC}$. The
613 126 heterozygous females were originally reported in Didion et al. (2015). Group
614 means were estimated using a linear mixed model with parity and genotype as
615 fixed effects and a random effect for each female using the lme4 package for R.
616 Confidence intervals were obtained by likelihood profiling and post-hoc
617 comparisons were performed via *F*-tests, using the Kenward-Roger
618 approximation for the effective degrees of freedom. The mean number of *R2d2*^{HC}
619 alleles transmitted per litter by heterozygous females with and without TRD was
620 estimated from data in Didion et al. (2015) with a weighted linear model, using
621 the total number of offspring per female as weights. Litter sizes are presented in
622 **Supplementary Table 2**, and estimates of group mean litter sizes in **Figure 3C**.

623 ***Whole-genome sequencing of HR selection lines.*** Ten individuals from
624 generation +61 of each of the eight HR selection lines were subject to whole-
625 genome sequencing. Briefly, high-molecular-weight genomic DNA was extracted
626 using a standard phenol/chloroform procedure. Illumina TruSeq libraries were
627 constructed using 0.5 µg starting material, with fragment sizes between 300 and
628 500 bp. Each library was sequenced on one lane of an Illumina HiSeq2000 flow
629 cell in a single 2x100bp paired-end run.

630 ***Null simulations of closed breeding populations.*** Widespread fixation of
631 alleles due to drift is expected in small, closed populations such as the HR lines
632 or the HR8xC57BL/6J advanced intercross line. But even in these scenarios, an
633 allele under positive selection is expected to fix 1) more often than expected by
634 drift alone in repeated breeding experiments using the same genetic
635 backgrounds, and 2) more rapidly than expected by drift alone. We used the R
636 package simcross (https://github.com/kbroman/simcross) to obtain the null
637 distribution of fixation times and fixation probabilities for an HR line under
638 Mendelian transmission.

639 We assume that the artificial selection applied for voluntary exercise in the HR
640 lines (described in Swallow *et al.* (1998)) was independent of *R2d2* genotype.
641 This assumption is justified for two reasons. First, 3 of 4 selection lines and 2 of 4
642 control (unselected) lines fixed $R2d2^{HC}$. Second, at the fourth and tenth
643 generation of the HR8xC57BL/6J advanced intercross, no quantitative trait loci
644 (QTL) associated with the selection criteria (total distance run on days 5 and 6 of
645 a 6-day trial) were found on Chromosome 2. QTL for peak and average running
646 speed were identified at positions linked to *R2d2*; however, HR8 alleles at those
647 QTL were associated with decreased, not increased, running speed (Kelly et al.
648 2010a; Leamy et al. 2012).

649 Without artificial selection an HR line reduces to an advanced intercross line
650 maintained by avoidance of sibling mating. We therefore simulated 100 replicates
651 of an advanced intercross with 10 breeding pairs and initial focal allele frequency
652 0.75. Trajectories were followed until the focal allele was fixed or lost. As a

653 validation we confirmed that the focal allele was fixed in 754 of 1000 runs, not
654 different from the expected 750 (p = 0.62, binomial test). Simulated trajectories
655 and the distribution of sojourn times are presented in **Figure 4B**.

656 The HR8xC57BL/6J advanced intercross line was simulated as a standard
657 biparental AIL with initial focal allele frequency of 0.5. Again, 1000 replicates of
658 an AIL with 20 breeding pairs were simulated and trajectories were followed until
659 the focal allele was fixed or lost. The result is presented in **Figure 4D**.

660 ***Investigation of population dynamics of meiotic drive.*** We used two
661 approaches to investigate the population dynamics of a female-limited meiotic
662 drive system with selection against the heterozygote. First, we evaluated the
663 fixation probability of a driving allele in relationship to transmission ratio (m),
664 selection coefficient against the heterozygote (s) and population size (N) by
665 modeling the population as a discrete-time Markov chain whose states are
666 possible counts of the driving allele. Define p_{t+1} to be the expected frequency of
667 the driving allele in generation t+1 given its frequency in the previous generation
668 (p_t). Following Hedrick et al. (1981), the expression for $p_{t+1}$is

$$p_{t+1} = \frac{(1-s)(1+2m)p_t(1-p_t) + 2(1-p_t)^2}{2[1-2sp_t(1-p_t)]}$$

669 In an infinite population, the equilibrium behavior of the system is governed by
670 the quantity q:

$$q = \frac{1}{2}(1-s)(1+2m)$$

671 When $q > 1$, the driving allele always increases in frequency. For values of $q \approx 1$
672 and smaller, the driving allele is either lost or reaches an unstable equilibrium
673 frequency determined m and s.

674 Let M be the matrix of transition probabilities for the Markov chain with 2N+1
675 states corresponding to possible counts of the driving allele in the population (0,
676 … 2N). The entries m_{ij} of M are

$$m_{ij} = \binom{2N}{i}(1-p_{t+1})^{2N-i}(p_{t+1})^i$$

677 Given a vector p_0 of starting probabilities, the probability distribution at generation
678 t is obtained by iteration:

$$p_t = p_0 M^t$$

679 We initiated the chain with a single copy of the driving allele (*i.e.* $p_0[1] = 1$).
680 Since this Markov chain has absorbing states (namely allele counts 0 and 2*N*),
681 we approximated steady-state probabilities by iterating the chain until the change
682 in probabilities between successive generations was < 10^{-4}. Fixation probability is
683 given by the value of the entry $p_t[2N]$ at convergence. We evaluated all possible
684 combinations of $0.5 \leq m \leq 1.0$ (in steps of 0.1) and $0 \leq s \leq 0.3$ (in steps of 0.05).

685 To investigate the effects of modifier loci on the frequency trajectory of a driving
686 allele we used forward-in-time simulations under a Wright-Fisher model with
687 selection, implemented in Python. Simulations assumed a constant population
688 size of *2N* = 200 chromosomes, each 100 cM long, with balanced sex ratio. At
689 the beginning of each run a driving allele was introduced (at 50 cM) on a single,
690 randomly chosen chromosome. Modifier alleles were introduced into the
691 population independently at a specified frequency, at position 0.5 cM (ie.
692 unlinked to the driving allele). To draw the next generation, an equal number of
693 male and female parents were selected (with replacement) from the previous
694 generation according to their fitness. Among females heterozygous for the driving
695 allele, transmission ratio (*m*) was calculated according to genotype at the
696 modifier loci (if any). For males and homozygous females, *m* = 0.5. Individuals
697 were assigned a relative fitness of 1 if *m* = 0.5 and 0.8 if *m* > 0.5. Recombination
698 was simulated under the Haldane model (*i.e.* a Poisson process along
699 chromosomes with no crossover interference). Finally, for each individual in the
700 next generation, one chromosome was randomly chosen from each parent with
701 probability *m*.

702 Simulation runs were restarted when the driving allele was fixed or lost, until 100
703 fixation events were observed in each condition of interest. Probability of fixation
704 was estimated using the waiting time before each fixation event, assuming a

705 geometric distribution of waiting times, using the fitdistr() function in the R
706 package MASS. Simulations are summarized in **Figure 5**.

707 Simulation code is available on GitHub:
708 https://github.com/andrewparkermorgan/r2d2-selfish-sweep.

709 References

710 Albrechtsen A, Moltke I, Nielsen R. 2010. Natural selection and the distribution of
711 identity-by-descent in the human genome. Genetics 186:295–308.

712 Babcock CS, Anderson WW. 1996. Molecular evolution of the Sex-Ratio
713 inversion complex in *Drosophila pseudoobscura*: analysis of the Esterase-5
714 gene region. Mol Biol Evol. 13:297–308.

715 Bersaglieri T, Sabeti PC, Patterson N, Vanderploeg T, Schaffner SF, Drake JA,
716 Rhodes M, Reich DE, Hirschhorn JN. 2004. Genetic signatures of strong
717 recent positive selection at the lactase gene. Am J Hum Genet. 74:1111–
718 1120.

719 Brandvain Y, Coop G. 2011. Scrambling eggs: meiotic drive and the evolution of
720 female recombination rates. Genetics 190:709–723.

721 Browning BL, Browning SR. 2013. Improving the accuracy and efficiency of
722 identity-by-descent detection in population data. Genetics 194:459–471.

723 Bryk J, Tautz D. 2014. Copy number variants and selective sweeps in natural
724 populations of the house mouse (*Mus musculus domesticus*). Front Genet.
725 5:153.

726 Collaborative Cross Consortium. 2012. The genome architecture of the
727 Collaborative Cross mouse genetic reference population. Genetics 190:389–
728 401.

729 Colonna V, Ayub Q, Chen Y, Pagani L, Luisi P, Pybus M, Garrison E, Xue Y,
730 Tyler-Smith C. 2014. Human genomic regions with exceptionally high levels
731 of population differentiation identified from 911 whole-genome sequences.
732 Genome Biol. 15:R88.

733 Derome N, Baudry E, Ogereau D, Veuille M, Montchamp-Moreau C. 2008.
734 Selective sweeps in a 2-locus model for sex-ratio meiotic drive in *Drosophila*
735 *simulans*. Mol Biol Evol. 25:409–416.

736 Derome N, Métayer K, Montchamp-Moreau C, Veuille M. 2004. Signature of
737 selective sweep associated with the evolution of sex-ratio drive in *Drosophila*
738 *simulans*. Genetics 166:1357–1366.

739 Didion JP, Morgan AP, Clayshulte AM-F, Mcmullan RC, Yadgary L, Petkov PM,
740 Bell TA, Gatti DM, Crowley JJ, Hua K, et al. 2015. A multi-megabase copy
741 number gain causes maternal transmission ratio distortion on mouse
742 chromosome 2. PLoS Genet. 11:e1004850.

743 Didion JP, Pardo-Manuel de Villena F. 2013. Deconstructing *Mus gemischus*:
744 advances in understanding ancestry, structure, and variation in the genome
745 of the laboratory mouse. Mamm. Genome 24:1–20.

746 Dyer KA, Charlesworth B, Jaenike J. 2007. Chromosome-wide linkage
747 disequilibrium as a consequence of meiotic drive. P Natl Acad Sci USA
748 104:1587–1592.

749 Esvelt KM, Smidler AL, Catteruccia F, Church GM, Tautz D. 2014. Concerning
750 RNA-guided gene drives for the alteration of wild populations. eLife Sciences
751 3:e03401.

752 Eversley CD, Clark T, Xie Y, Steigerwalt J, Bell TA, de Villena FP, Threadgill
753 DW. 2010. Genetic mapping and developmental timing of transmission ratio
754 distortion in a mouse interspecific backcross. BMC Genet. 11:98.

755 Fariello MI, Boitard S, Naya H, SanCristobal M, Servin B. 2013. Detecting
756 signatures of selection through haplotype differentiation among hierarchically
757 structured populations. Genetics 193:929–941.

758 Fishman L, Saunders A. 2008. Centromere-associated female meiotic drive
759 entails male fitness costs in monkeyflowers. Science 322:1559–1562.

760 Fu W, Akey JM. 2013. Selection and adaptation in the human genome. Annu
761 Rev Genomics Hum Genet. 14:467–489.

762 Gantz VM, Bier E. 2015. The mutagenic chain reaction: a method for converting
763 heterozygous to homozygous mutations. Science 348:442–444.

764 Geraldes A, Basset P, Smith KL, Nachman MW. 2011. Higher differentiation
765 among subspecies of the house mouse (*Mus musculus*) in genomic regions
766 with low recombination. Mol Ecol. 20:4722–4736.

767 Gillespie JH. 2010. Population genetics: a concise guide. 2nd ed. Baltimore: JHU
768 Press.

769 Grossman SR, Andersen KG, Shlyakhter I, Tabrizi S, Winnicki S, Yen A, Park
770 DJ, Griesemer D, Karlsson EK, Wong SH, et al. 2013. Identifying recent
771 adaptations in large-scale genomic data. Cell 152:703–713.

772 Hammond A, Galizi R, Kyrou K, Simoni A, Siniscalchi C, Katsanos D, Gribble M,
773 Baker D, Marois E, Russell S, et al. 2015. A CRISPR-Cas9 gene drive
774 system targeting female reproduction in the malaria mosquito vector

775 *Anopheles gambiae*. Nat Biotechnol. online ahead of print.

776 Hartl DL. 1973. Complementation analysis of male fertility among the segregation
777 distorter chromosomes of *Drosophila melanogaster*. Genetics 73:613–629.

778 Hedrick PW. 1981. The establishment of chromosomal variants. Evolution
779 35:322–332.

780 Henikoff S, Malik HS. 2002. Centromeres: selfish drivers. Nature 417:227–227.

781 Hernandez RD, Kelley JL, Elyashiv E, Melton SC, Auton A, McVean GAT, 1000
782 Genomes Project Consortium, Sella G, Przeworski M. 2011. Classic selective
783 sweeps were rare in recent human evolution. Science 331:920–924.

784 Kaplan NL, Hudson RR, Langley CH. 1989. The “hitchhiking effect” revisited.
785 Genetics 123:887–899.

786 Kelly SA, Nehrenberg DL, Peirce JL, Hua K, Steffy BM, Wiltshire T, Pardo-
787 Manuel de Villena F, Garland T, Pomp D. 2010a. Genetic architecture of
788 voluntary exercise in an advanced intercross line of mice. Physiol. Genomics
789 42:190–200.

790 Kelly SA, Nehrenberg DL, Hua K, Gordon RR, Garland T, Pomp D. 2010b.
791 Parent-of-origin effects on voluntary exercise levels and body composition in
792 mice. Physiol. Genomics 40:111–120.

793 Kingan SB, Garrigan D, Hartl DL. 2010. Recurrent selection on the Winters sex-
794 ratio genes in *Drosophila simulans*. Genetics 184:253–265.

795 Laurie CC, Nickerson DA, Anderson AD, Weir BS, Livingston RJ, Dean MD,
796 Smith KL, Schadt EE, Nachman MW. 2007. Linkage disequilibrium in wild
797 mice. PLoS Genet. 3:e144.

798 Leamy LJ, Kelly SA, Hua K, Pomp D. 2012. Exercise and diet affect quantitative
799 trait loci for body weight and composition traits in an advanced intercross
800 population of mice. Physiol. Genomics 44:1141–1153.

801 Li H, Handsaker B, Wysoker A, Fennell T, Ruan J, Homer N, Marth G, Abecasis
802 G, Durbin R, 1000 Genome Project Data Processing Subgroup. 2009. The
803 Sequence Alignment/Map format and SAMtools. Bioinformatics 25:2078–
804 2079.

805 Liu EY, Morgan AP, Chesler EJ, Wang W, Churchill GA, Pardo-Manuel de
806 Villena F. 2014. High-resolution sex-specific linkage maps of the mouse
807 reveal polarized distribution of crossovers in male germline. Genetics
808 197:91–106.

809 Liu EY, Zhang Q, McMillan L, Pardo-Manuel de Villena F, Wang W. 2010.

810 Efficient genome ancestry inference in complex pedigrees with inbreeding.
811 Bioinformatics 26:i199–i207.

812 Lyon MF. 1991. The genetic basis of transmission-ratio distortion and male
813 sterility due to the *t* complex. The American Naturalist 137:349–358.

814 Maynard Smith J, Haigh J. 1974. The hitch-hiking effect of a favourable gene.
815 Genet Res. 23:23–35.

816 Montagutelli X, Turner R, Nadeau JH. 1996. Epistatic control of non-Mendelian
817 inheritance in mouse interspecific crosses. Genetics 143:1739–1752.

818 Morgan AP, Fu C-P, Kao C-Y, Welsh CE, Didion JP, Yadgary L, Hyacinth L,
819 Ferris MT, Bell TA, Miller DR, et al. 2015. The Mouse Universal Genotyping
820 Array: From Substrains to Subspecies. G3 online ahead of print.

821 Morgan AP, Welsh CE. 2015. Informatics resources for the Collaborative Cross
822 and related mouse populations. Mamm. Genome 26:521-539.

823 Nolte V, Pandey RV, Kofler R, Schlötterer C. 2013. Genome-wide patterns of
824 natural variation reveal strong selective sweeps and ongoing genomic conflict
825 in *Drosophila mauritiana*. Genome Res. 23:99-110.

826 Pardo-Manuel de Villena F, Sapienza C. 2001. Female meiosis drives karyotypic
827 evolution in mammals. Genetics 159:1179–1189.

828 Pardo-Manuel de Villena F. 2004. Evolution of the mammalian karyotype. In:
829 Ruvinsky A, Graves JAM, editors. Mammalian Genomics. Cambridge (MA):
830 CABI Publishing. p. 317–348.

831 Pelz H-J, Rost S, Hünerberg M, Fregin A, Heiberg A-C, Baert K, MacNicoll AD,
832 Prescott CV, Walker A-S, Oldenburg J, et al. 2005. The genetic basis of
833 resistance to anticoagulants in rodents. Genetics 170:1839–1847.

834 Pezer Ž, Harr B, Teschke M, Babiker H, Tautz D. 2015. Divergence patterns of
835 genic copy number variation in natural populations of the house mouse (*Mus*
836 *musculus domesticus*) reveal three conserved genes with major population-
837 specific expansions. Genome Res. 25:1114-1124.

838 Pickrell JK, Pritchard JK. 2012. Inference of population splits and mixtures from
839 genome-wide allele frequency data. PLoS Genet. 8:e1002967.

840 Pocock M, Hauffe HC, Searle JB. 2005. Dispersal in house mice. Bio J Linn Soc.
841 84:565–583.

842 Presgraves DC, Gérard PR, Cherukuri A, Lyttle TW. 2009. Large-scale selective
843 sweep among segregation distorter chromosomes in African populations of
844 *Drosophila melanogaster*. PLoS Genet. 5:e1000463.

845 Purcell S, Neale B, Todd-Brown K, Thomas L, Ferreira MA, Bender D, Maller J,
846 Sklar P, de Bakker PI, Daly MJ, et al. 2007. PLINK: a tool set for whole-
847 genome association and population-based linkage analyses. Am J Hum
848 Genet. 81:559–575.

849 Rogala AR, Morgan AP, Christensen AM, Gooch TJ, Bell TA, Miller DR, Godfrey
850 VL, Pardo-Manuel de Villena F. 2014. The Collaborative Cross as a resource
851 for modeling human disease: CC011/Unc, a new mouse model for
852 spontaneous colitis. Mamm. Genome 25:95–108.

853 Sabeti PC, Reich DE, Higgins JM, Levine HZP, Richter DJ, Schaffner SF, Gabriel
854 SB, Platko JV, Patterson NJ, McDonald GJ, et al. 2002. Detecting recent
855 positive selection in the human genome from haplotype structure. Nature
856 419:832–837.

857 Sandler L, Novitski E. 1957. Meiotic drive as an evolutionary force. American
858 Naturalist 91:105–110.

859 Scheet P. 2006. A fast and flexible statistical model for large-scale population
860 genotype data: applications to inferring missing genotypes and haplotypic
861 phase. Am J Hum Genet. 78:629–644.

862 Siracusa LD, Alvord WG, Bickmore WA, Jenkins NA, Copeland NG. 1991.
863 Interspecific backcross mice show sex-specific differences in allelic
864 inheritance. Genetics 128:813–821.

865 Song Y, Endepols S, Klemann N, Richter D, Matuschka F-R, Shih C-H, Nachman
866 MW, Kohn MH. 2011. Adaptive introgression of anticoagulant rodent poison
867 resistance by hybridization between old world mice. Curr Biol. 21:1296–1301.

868 Staubach F, Lorenc A, Messer PW, Tang K, Petrov DA, Tautz D. 2012. Genome
869 patterns of selection and introgression of haplotypes in natural populations of
870 the house mouse (*Mus musculus*). PLoS Genet 8:e1002891.

871 Stephens JC, Reich DE, Goldstein DB, Shin HD, Smith MW, Carrington M,
872 Winkler C, Huttley GA, Allikmets R, Schriml L, et al. 1998. Dating the origin of
873 the CCR5-Delta32 AIDS-resistance allele by the coalescence of haplotypes.
874 Am J Hum Genet. 62:1507–1515.

875 Stevens EL, Heckenberg G, Roberson EDO, Baugher JD, Downey TJ, Pevsner
876 J. 2011. Inference of relationships in population data using identity-by-
877 descent and identity-by-state. PLoS Genet. 7:e1002287.

878 Svenson KL, Gatti DM, Valdar W, Welsh CE, Cheng R, Chesler EJ, Palmer AA,
879 McMillan L, Churchill GA. 2012. High-resolution genetic mapping using the
880 Mouse Diversity outbred population. Genetics 190:437–447.

881 Swallow JG, Carter PA, Garland T Jr. 1998. Artificial selection for increased

882 wheel-running behavior in house mice. Behavior Genetics 28:227–237.

883 Szpiech ZA, Hernandez RD. 2014. selscan: an efficient multithreaded program to
884 perform EHH-based scans for positive selection. Mol Biol Evol. 31:2824–
885 2827.

886 Voight BF, Kudaravalli S, Wen X, Pritchard JK. 2006. A map of recent positive
887 selection in the human genome. PLoS Biol 4:e72.

888 White MJD. 1978. Modes of Speciation. 1st ed. San Francisco: W.H.Freeman &
889 Co Ltd.

890 Williamson SH, Hubisz MJ, Clark AG, Payseur BA, Bustamante CD, Nielsen R.
891 2007. Localizing recent adaptive evolution in the human genome. PLoS
892 Genet. 3:e90.

893 Yang H, Wang JR, Didion JP, Buus RJ, Bell TA, Welsh CE, bonhomme F, Yu
894 AH-T, Nachman MW, Piálek J, et al. 2011. Subspecific origin and haplotype
895 diversity in the laboratory mouse. Nat Genet. 43:648–655.

Acknowledgements

We wish to thank all the scientists and research personnel who collected and processed the samples used in this study. In particular we acknowledge Luanne Peters and Alex Hong-Tsen Yu for providing critical samples; Ryan Buus and T. Justin Gooch for isolating DNA for high-density genotyping of wild-caught mice; and Vicki Cappa, A. Cerveira, Daniel Förster, Guila Ganem, Ron and Annabelle Lesher, K. Saïd, Toni Schelts, Dan Small, and J. Tapisso for aiding in mouse trapping. We thank Muriel Davisson at the Jackson Laboratory for maintaining, for several decades, tissue samples from breeding colonies used to generate wild-derived inbred strains. We also thank Francis Collins, Jim Evans, Matthew Hahn, and Corbin Jones for comments on an earlier version of this manuscript. This work was supported by the National Institutes of Health T32GM067553 to JPD and APM, F30MH103925 to APM, P50GM076468 to EJC, GAC, and FPMV, K01MH094406 to JJC, DK-076050 and DK-056350 to DP, AG038070 to GAC, and the intramural research program to BR and SPR; National Science Foundation IOS-1121273 to TG; Vaadia-BARD Postdoctoral Fellowship Award FI-478-13 to LY; U.S. Army Medical Research and Materiel Command W81XWH-11-1-0762 to CJB; The Jackson Laboratory new investigator funds to EJC; The National Center for Scientific Research, France to JBD (This is contribution n°ISEM 2016-002); the University of Rome “La Sapienza” to RC and ES; Claraz-Stiftung to AL; Natural Environment Research Council (UK) to MDG, HCH and JBS; EU Human Capital and Mobility Programme (CHRX-CT93-0192) to HCH and JBS; Foundation for Science and Technology, Portugal PTDC/BIA-EVF/116884/2010 and UID/AMB/50017/2013 to SIG, MLM and JBS; Spanish "Ministerio de Ciencia y Tecnología” CGL2007-62111 and "Ministerio de Economía y Competitividad” CGL2010-15243 to JV; and the Oliver Smithies Investigator funds provided by the School of Medicine at University of North Carolina to FPMV.

Author Contributions

JPD, GAC and FPMV conceived the study. JBD, CJB, KJC, RC, Y-HC, AJC, JJC, EJC, JEF, SIG, DMG, TG, EBG-A, MDG, SAG, IG, AH, HCH, JSH, JMH, KH, WJJ, AKL, MJL-F, GM, MM, LM, MGR, BR, SPR, JBS, MSS, ES, KLS, PT-L, DWT, JVQ, GMW, DP, GAC, and FPMV provided biological samples and/or unpublished data sets. APM, LY, TAB, RCM, and LOdS conducted experiments. JPD, APM, and LY analyzed the data. JPD, APM, and FPMV wrote the paper.

Author Information

All data is made available at http://csbio.unc.edu/r2d2/. The authors declare no competing financial interests. Correspondence and requests for materials should be addressed to FPMV (fernando@med.unc.edu).

937 **Figure Legends**

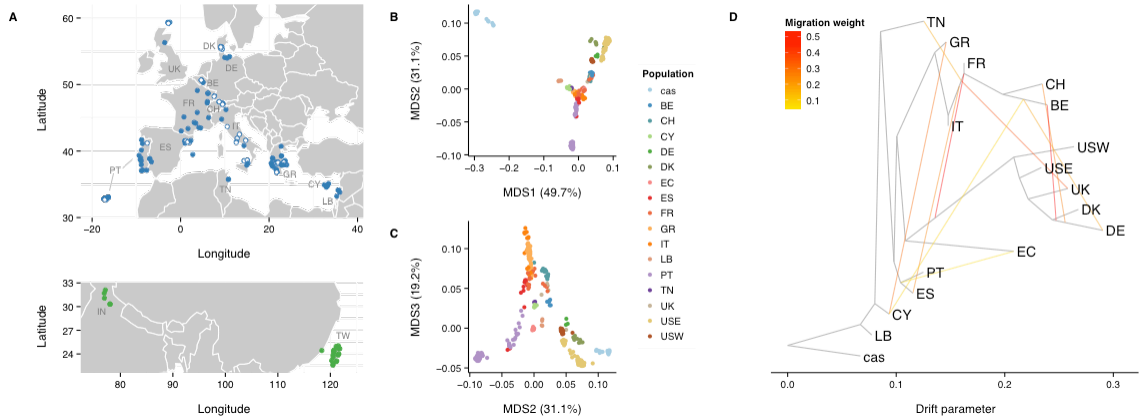

938

939 **Figure 1. Wild mouse populations used in this study. (A)** Geographic
940 distribution of samples used in this study. Samples are colored by taxonomic
941 origin: blue for *M. m. domesticus*, green for *M. m. castaneus*. Those with
942 standard karyotype (2*n* = 40) are indicated by closed circles; samples with
943 Robertsonian fusion karyotypes (2*n* < 40) are indicated by open circles.
944 Populations from Floreana Island (Galapagos Islands, Ecuador; "EC"), Farallon
945 Island (off the coast of San Francisco, California, United States; "USW"), and
946 Maryland, United States ("USE") are not shown. **(B,C)** Multidimensional scaling
947 (MDS) (*k* = 3 dimensions) reveals population stratification consistent with
948 geography. *M. m. domesticus* populations are labeled by country of origin.
949 Outgroup samples of *M. m. castaneus* origin are combined into a single cluster
950 ("cas"). **(D)** Population graph estimated from autosomal allele frequencies by
951 TreeMix. Black edges indicate ancestry, while red edges indicate gene flow by
952 migration or admixture. Topography of the population graph is consistent with
953 MDS result and with the geographic origins of the samples.

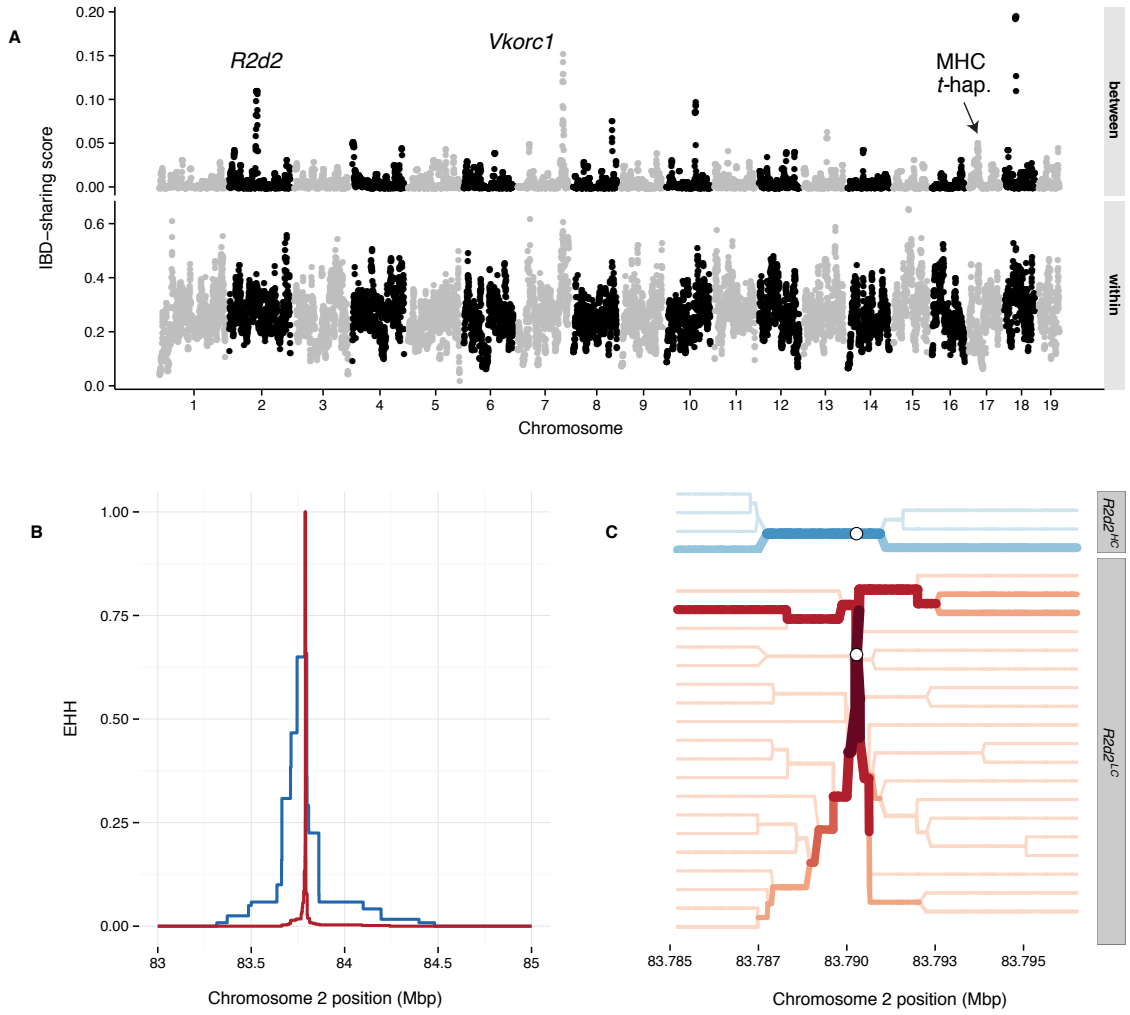

954

955 **Figure 2. Haplotype-sharing at *R2d2* provides evidence of a selective**
956 **sweep in wild mice of European origin. (A)** Weighted haplotype-sharing score
957 (see **Online Methods**), computed in 500 kb bins across autosomes, when those
958 individuals are drawn from the same population (lower panel) or different
959 populations (upper panel). Peaks of interest overlay *R2d2* (Chromosome 2; see
960 **Supplementary Figure 2** for zoomed-in view) and *Vkorc1* (distal Chromosome
961 7). The position of the closely linked *t*-haplotype and MHC loci is also marked.
962 **(B)** Decay of extended haplotype homozygosity (EHH) (Sabeti et al. 2002) on the
963 $R2d2^{HC}$-associated (blue) versus the $R2d2^{LC}$-associated (red) haplotype. EHH is
964 measured outward from the index SNP at chr2:83,790,275 and is bounded
965 between 0 and 1. **(C)** Haplotype bifurcation diagrams for the $R2d2^{HC}$ (top panel,
966 red) and $R2d2^{LC}$ (bottom panel, blue) haplotypes at the index SNP (open circle).

967 Darker colors and thicker lines indicate higher haplotype frequencies. Haplotypes
968 extend 100 sites in each direction from the index SNP.

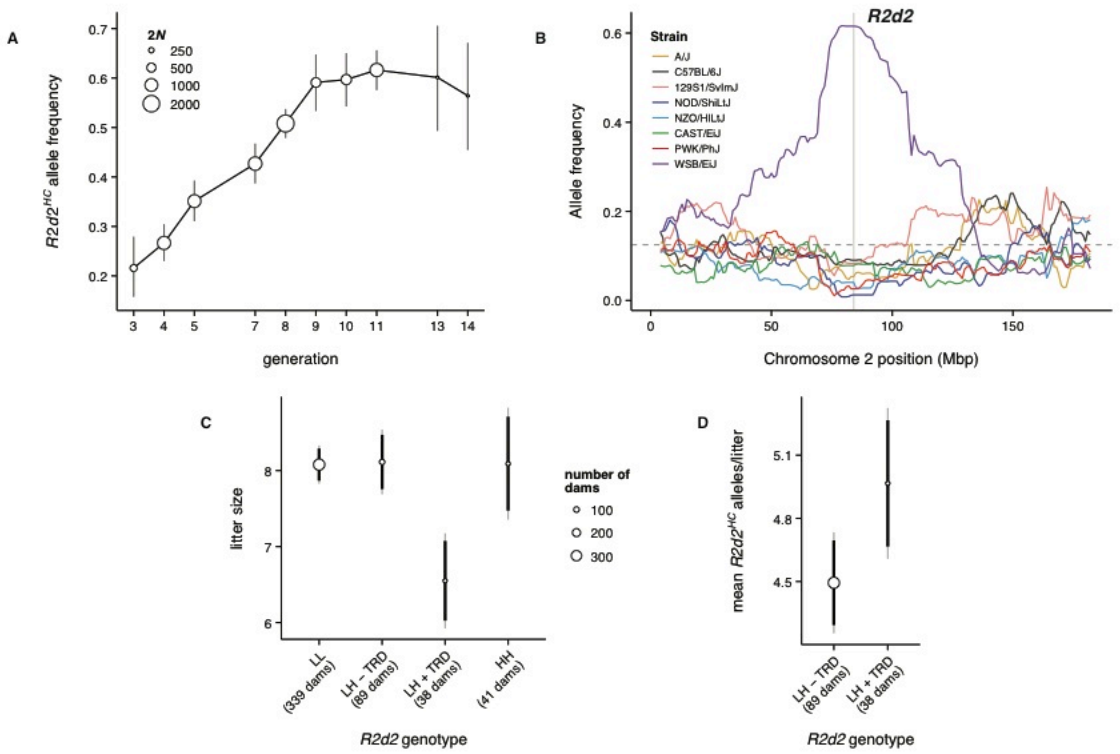

969

970 **Figure 3. An *R2d2^{HC}* allele rises to high frequency despite negative effect**
971 **on litter size in the DO. (A)** *R2d2* drives three-fold increase in WSB/EiJ allele
972 frequency in 13 generations in the DO population. Circle sizes reflect number of
973 chromosomes genotyped (2*N*); error bars are +/- 2 SE. **(B)** Allele frequencies
974 across Chromosome 2 (averaged in 1 Mb bins) at generation 13 of the DO,
975 classified by founder strain. Grey shaded region is the candidate interval for
976 *R2d2*. **(C)** Mean litter size among DO females according to *R2d2* genotype: LL,
977 *R2d2$^{LC/LC}$*; LH – TRD, *R2d2$^{LC/HC}$* without transmission ratio distortion; LH + TRD,
978 *R2d2$^{LC/HC}$* with transmission ratio distortion; HH, *R2d2$^{HC/HC}$*. Circle sizes reflect
979 number of females tested; error bars are 95% confidence intervals from a linear
980 mixed model which accounts for parity and repeated measures on the same
981 female (see **Methods**.) **(D)** Mean absolute number of *R2d2^{HC}* alleles transmitted
982 in each litter by heterozygous females with (LL + TRD) or without (LL – TRD)

983 transmission ratio distortion. LL + TRD females transmit more *R2d2*^{HC} alleles
984 despite their significantly reduced litter size.

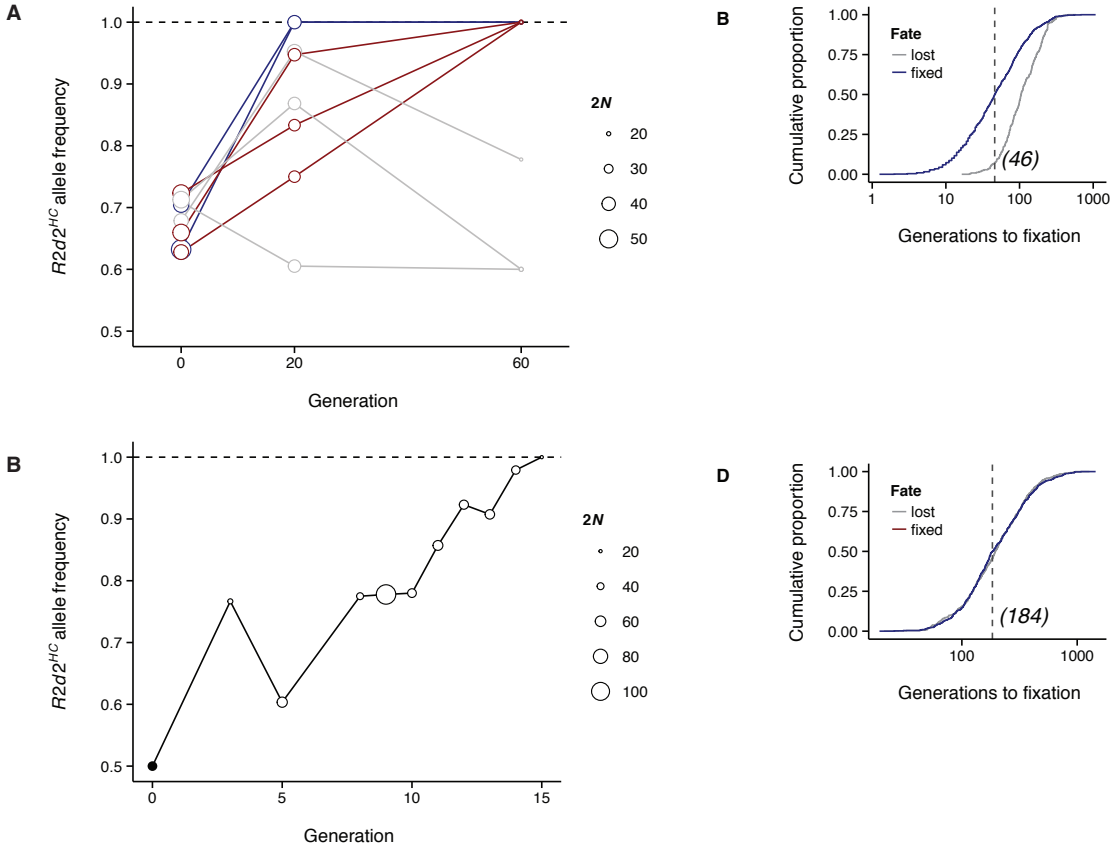

985

986 **Figure 4. *R2d2*^{HC} alleles rapidly increase in frequency in ICR:Hsd-derived**
987 **laboratory populations. (A)** *R2d2*^{HC} allele frequency during breeding of 4 HR
988 selection lines and 4 control lines. Trajectories are colored by their fate: blue,
989 *R2d2*^{HC} fixed by generation 20; red. *R2d2*^{HC} fixed by generation 60; grey, *R2d2*^{HC}
990 not fixed. Circle sizes reflect number of chromosomes (*2N*) genotyped. **(B)**
991 Cumulative distribution of time to fixation (blue) or loss (grey) of the focal allele in
992 1,000 simulations of an intercross line mimicking the HR breeding scheme.
993 Dotted line indicates median fixation time. **(C)** *R2d2*^{HC} allele frequency during
994 breeding of an (HR8xC57BL/6J) advanced intercross line. Circle sizes reflect
995 number of chromosomes (*2N*) genotyped. **(D)** Cumulative distribution of time to
996 fixation (blue) or loss (grey) of the focal allele in 1,000 simulations of an

997 advanced intercross line mimicking the HR8xC57BL/6J AIL. Dotted line indicates
998 median fixation time.

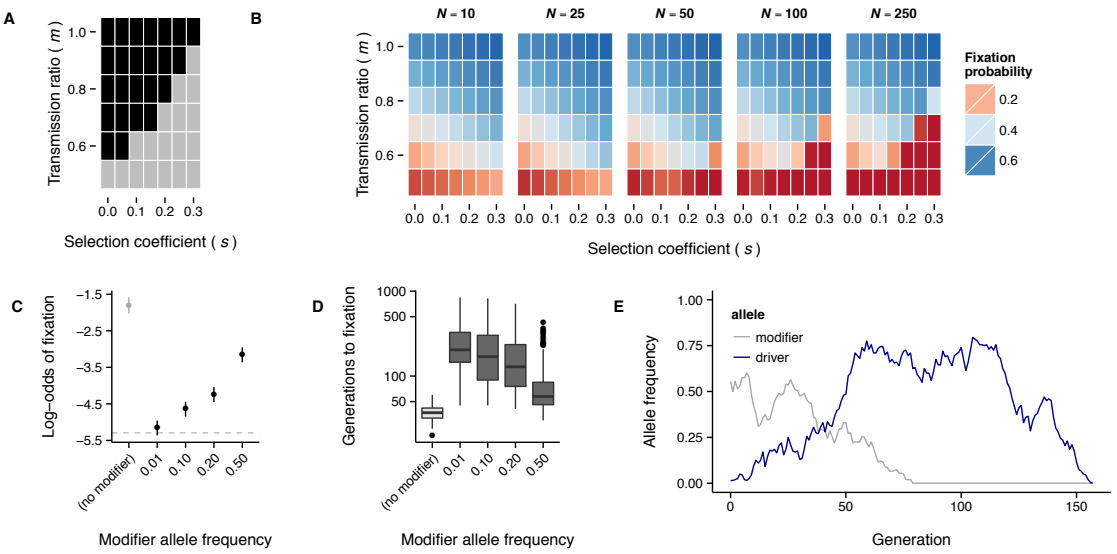

999

1000 **Figure 5. Population dynamics of a meiotic drive allele. (A)** Phase diagram
1001 for a meiotic drive system like *R2d2*, with respect to transmission ratio (*m*) and
1002 selection coefficient against the heterozygote (*s*). Regions of the parameter
1003 space for which there is directional selection for the driving allele are shown in
1004 black; regions in which there are unstable equilibria or directional selection
1005 against the driving allele are shown in grey. **(B)** Probability of fixing the driving
1006 allele as a function of *m*, *s* and population size (*N*). Notice that, in the area
1007 corresponding to the grey region of panel A, fixation probability declines rapidly
1008 as population size increases. **(C)** Probability of fixing the driving allele in
1009 simulations of meiotic drive dependent on a single modifier locus (*N* = 100, *s* =
1010 0.2, maximum *m* = 0.8, initial driver frequency 1/2*N*). Estimates are given +/- 2
1011 SE. Grey dashed line corresponds to fixation probability for a neutral allele
1012 (1/2*N*). **(D)** Time to fixation of the driving allele. Values represent 100 fixation
1013 events in each condition. **(E)** Example allele-frequency trajectories from a
1014 "collapsed" selfish sweep: while the modifier allele is present at intermediate
1015 frequency, the driving allele sweeps to a frequency of ~ 0.75. After the modifier
1016 allele is lost, the driver drifts out of the population as well.

1017 **Table 1. *R2d2*^{HC} allele frequencies in wild *M. m. domesticus* populations.**

1018 **Table 1. *R2d2^{HC}* allele frequencies in wild *M. m. domesticus* populations.**

Population	R2d2HC Allele Freq	2 x (Number of Individuals)
BE	0.50	6
CH	0.32	28
CY	0.00	14
DE	0.67	6
DK	0.06	18
EC	0.00	24
ES	0.22	18
FR	0.15	26
GR	0.08	106
IT	0.09	34
LB	0.25	8
PT	0.13	54
TN	0.00	4
UK	0.00	6
USE	0.21	102
USW	0.00	24

1019